Numerical simulation of low-velocity impact loading of polymeric materials

H. Daiyan[1], F. Grytten[1], E. Andreassen[1], O.V. Lyngstad[2], H. Osnes[3,4], R.H. Gaarder[1] and E.L. Hinrichsen[1]

[1] SINTEF Materials and Chemistry, Box 124 Blindern, NO-0314 Oslo, Norway
[2] Plastal AS, Box 94, NO-2831 Raufoss, Norway
[3] Dept. of Mathematics, University of Oslo, Box 1053 Blindern, NO-0316 Oslo, Norway
[4] Simula Research Laboratory, Box 134, NO-1325 Lysaker, Norway
E-mail: hamid.daiyan@sintef.no

Summary:

Simulation of ductile polymers subjected to impact loading has become an important topic [1, 2], especially for automotive components related to passenger and pedestrian safety. The aim of our work is to establish and validate numerical models for impact response, and this presentation will focus on a study of impact on injection molded polypropylene plates.

SAMP-1 (Semi-Analytical Model for Polymers) [3] was selected as constitutive model in LS-DYNA. This model takes tabulated data from experiments as input, and includes strain rate effects, pressure sensitive plasticity, plastic volume dilatation and damage. As the material behavior is complex, and data for large strains are needed, a major task is to obtain reliable data from material tests.

Uniaxial tension and uniaxial compression tests were performed to calibrate the constitutive model. Three-dimensional digital image correlation (3D-DIC) [4] with two cameras and stereo vision was used to determine full-field displacements during uniaxial tensile tests, in order to quantify plastic volumetric strains and to obtain true stress-strain curves (the isochoric assumption is invalid for the present material). Uniaxial compression tests were made with short specimens in order to avoid buckling.

Falling weight impact of plates (centrally loaded, circular clamping) and bars (three-point bending), and quasi-static three-point bending of bars, were simulated. Measured force vs. displacement, and permanent deformation of plates, were compared to numerical predictions. Figure 1 shows results for falling weight impact of a 4 mm thick plate. SAMP-1 is suitable for such materials, but improved material data are needed for e.g. strain rate effects and stress state effects.

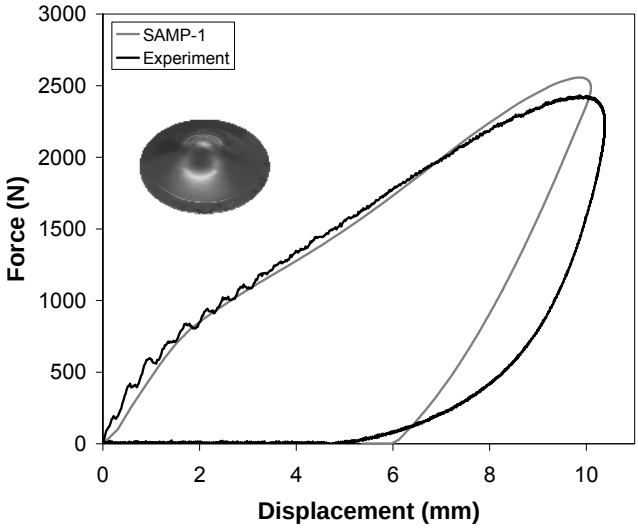

Figure 1: Falling weight impact results for 4 mm thick plate (impact velocity 3 m/s, temperature 23 °C).

Keywords:
Impact, Polypropylene, LS-DYNA, SAMP-1, DIC

1. Introduction

Numerical simulation of impact loading of polymer materials is of great industrial interest, as these materials are increasingly being used in critical applications and structures. The response to impact loads is of particular interest for automotive applications related to passenger and pedestrian safety. Hence, the automotive industry is a driving force in this field. Constitutive models used for these materials today have shortcomings when it comes to predicting multiaxial loading, unloading response (rebound), and fracture.

Ductile polymeric materials show a complex behavior in impact loading involving large strains. The complexity applies to the micromechanical mechanisms as well as the macroscopic response. Therefore, more complex constitutive models are needed, requiring material input which is difficult to determine experimentally.

2. Experimental

Accurate and reliable experimental results are needed to calibrate the constitutive model in order to obtain reliable numerical predictions. Materials with a complex yield function, such as polymers, should be tested in different stress states, such as uniaxial tension, biaxial tension, uniaxial compression and shear. At the same time, results should be obtained for large strains and high strain rates, and at relevant temperatures. Damage evolution should also be characterized in order to accurately predict rebound or spring back. Thus, several material tests are needed to fully characterize the parameters of the constitutive model. On the other hand, engineers would like to use as few and simple tests as possible in calibration.

The anisotropy and inhomogeneity of injection molded parts can be a challenge when trying to predict their mechanical response [5]. Quasi-static three-point bending tests were performed on bars machined from injection-molded dogbones (ISO 527-2, specimen type 1A) and from plates (4×80×80 mm^3). Bars were cut in directions parallel and perpendicular to the flow direction in the plates. All the bars had the same nominal dimensions (4×10×80 mm^3, where 4 mm is the original thickness of the injection moulded parts). As shown in Figure 2, the plate is anisotropic in the plane. As often reported, the stiffness is higher in the flow direction. The bar cut from the dogbone has a response similar to the bar from the flow direction in the plate at low deflections. The difference at larger deflections could be caused by material anisotropy, but also by heterogeneous mechanical properties. The dogbones were injection moulded with processing parameters based on ISO 294-1 and ISO 1873-2, and similar parameters were used for the plates. Effects of processing parameters will be the subject of a separate study.

The material in this study is a commercial 20% mineral and elastomer modified polypropylene compound (PP+EPDM-TD20) for injection-molded automotive exterior parts. All tests were performed at 23 °C.

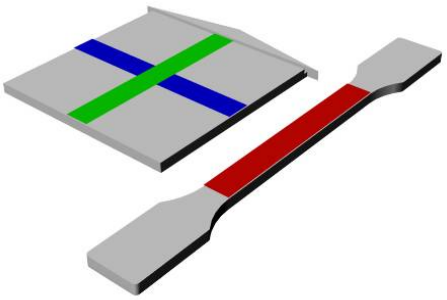

Injection moulded plate and dogbone and illustration of bars machined from these parts.

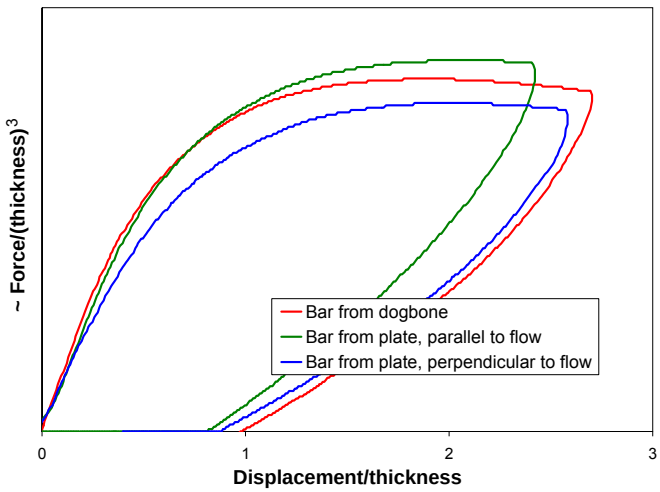

Figure 2: Experimental results for three-point bending of bars machined from injection moulded parts. Loading rate: 10 mm/min. The dogbones were ca. 0.2 mm thicker than the plates, hence the scaling of the force in the diagram (which of course only is valid up to a certain displacement).

2.1 Calibration tests

Uniaxial tension and uniaxial compression tests were performed to calibrate the constitutive model. 3D digital image correlation (DIC) was used in the tensile measurements. Two digital cameras were placed so that both recorded the same two sides of the specimen simultaneously (Figure 3). The average logarithmic strain in the longitudinal direction in any cross section, ε_{xx}, can be calculated from the average Green-Lagrange strain in that cross-section, $\overline{E}_{xx}$, as

$$\varepsilon_{xx} = \frac{1}{2}\ln\left(1+2\overline{E}_{xx}\right) \tag{1}$$

If the stresses and strains are assumed to be uniform over each cross section, the Cauchy stress, σ_{xx}, can be expressed as

$$\sigma_{xx} = \frac{F}{A} = \frac{F}{A_0}\frac{A_0}{A} = \frac{F}{A_0}\frac{w_0}{w}\frac{t_0}{t} = \frac{F}{A_0}\frac{1}{\sqrt{1+2\overline{E}_{yy}}\sqrt{1+2\overline{E}_{zz}}} \tag{2}$$

Where F is the current force, A and A_0 are the current and initial cross-sectional areas, w and w_0 are the current and initial specimen widths, and t and t_0 are the current and initial specimen thicknesses, respectively.

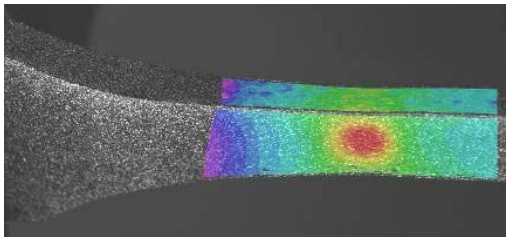

Figure 3: Contours of longitudinal strain in the area of interest of the dogbone. Test speed 10 mm/min.

Tensile tests at two different cross-head speeds, 10 and 100 mm/min (nominal strain rates of 0.002 s^{-1} and 0.02 s^{-1}), were performed with both DIC and a conventional extensometer. The hardening curves at these two rates had similar shapes, see Figure 4. For our simulations, the hardening curve obtained using DIC at 10 mm/min was scaled and used as input for all strain rates. A comparison between stress-strain curves obtained with DIC and with a extensometer (assuming isochoric deformation) showed good agreement up to the yield point. After some yielding, the constant volume assumption lead to an overestimation of the stress. Since a good agreement was observed between extensometer based and DIC based data up to the yield point, tests were conducted at elevated strain rates (0.1, 12.5 and 125 s^{-1}) using only the extensometer. Yield stress vs. strain rate was determined, and the quasi-static hardening curve was scaled accordingly. In addition, a test at 0.0002 s^{-1} was carried out. The scaling of the yield stress was found to be almost linear on a logarithmic scale (Figure 4). At the highest strain rate (125 s^{-1}, corresponding to a loading rate of 10 m/s), the yield stress has rather large experimental scatter due to dynamic effects. Poisson's ratio versus total strain is shown in Figure 5. It was calculated from transverse and longitudinal strains measured with DIC.

Uniaxial tensile loading-unloading tests, with unloading from different displacements, were used to determine a damage parameter. All tests were done at 10 mm/min and the cross-head speed was kept constant during loading and unloading. A simple damage parameter [6] can be defined from the reduction in stiffness when comparing the effective modulus during unloading with the initial modulus:

$$D = 1 - \frac{E_{unloading}}{E_0} \tag{3}$$

Figure 6 shows the loading-unloading curves, as well as the damage parameter vs. plastic strain determined from these curves. A double-term exponential function was used to fit the data:

$$D(\varepsilon^p) = ae^{b\varepsilon^p} + ce^{d\varepsilon^p} \quad (4)$$

with constants a = 0.8854, b = 0.0681, c = -0.8841 and d = -58.88.

For polymer materials, the yield stress in compression is usually higher than that in tension. Specimens for uniaxial compression tests were machined from the middle of the dogbones. Specimens with dimensions recommended by ISO 604 for compressive strength measurements (10 mm high, cross-section 4×10 mm^2) buckled at nominal strains of ca 0.25. Specimen with smaller dimensions (4×4×4 mm^3 [7]) were tested at 2 mm/min, and for these specimens barreling occurred at a strain of ca 0.5. The cross-head displacement and the force were used to find nominal strains and stresses. The nominal yield stresses were practically the same with the two different specimen dimensions. The contact surfaces were lubricated with PTFE tape and soap water [7].

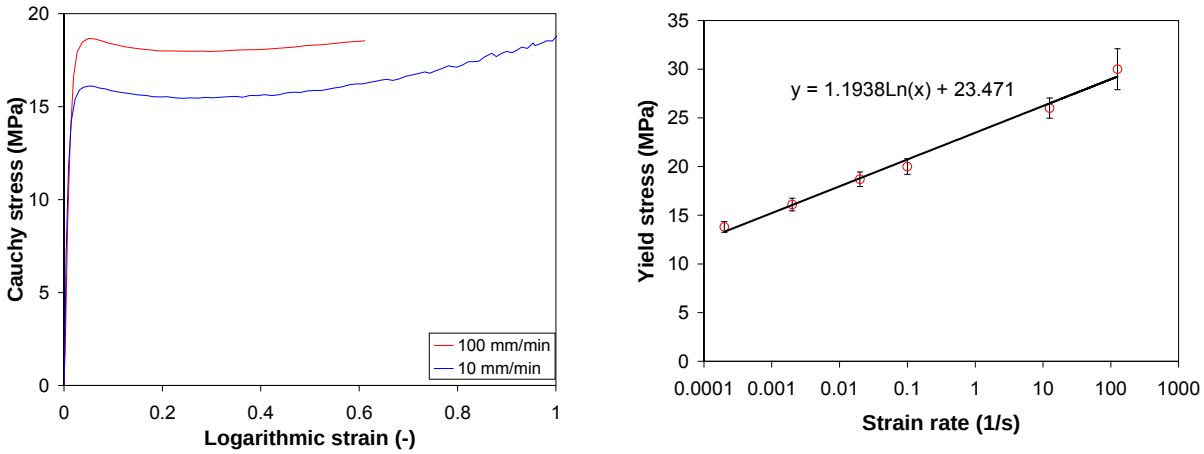

Figure 4: Left*: True tensile strain-stress curve for two different cross-head speeds.* Right*: Yield stress versus strain rate.*

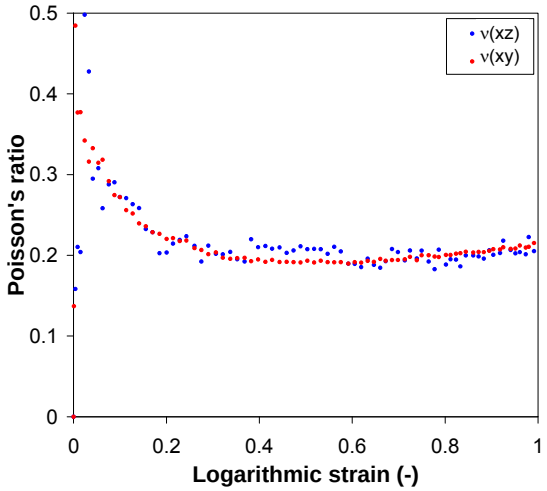

Figure 5: Poisson's ratio versus total strain in both transverse directions. The symbols $\nu(xz)$ *and in* $\nu(xy)$ *the legend denote the Poisson's ratios for the 4 mm and 10 mm wide sides of the specimen, respectively. Test speed 10 mm/min.*

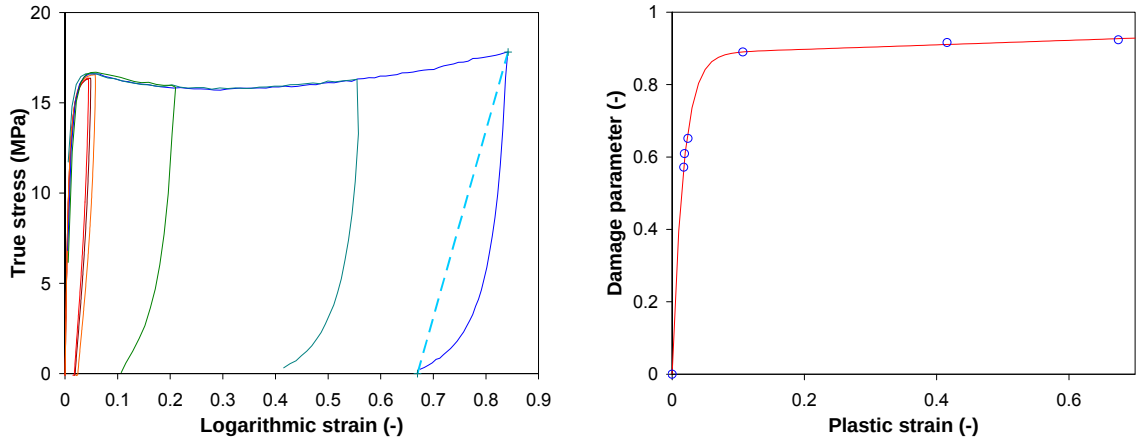

Figure 6: Left: Uniaxial tensile loading-unloading curves. Right: Damage parameter versus plastic strain (circles) and exponential fitted curve (line).

2.2 Validation tests

Two series of tests were selected for comparison with numerical simulations.

A) Falling weight impact on plate

Fully clamped 2 and 4 mm thick plates were subjected to impact loading. The outer and inner diameters of the clamping were 60 and 40 mm, respectively. A hemispherical striker with 20 mm diameter was used. The striker was lubricated with silicone grease. The impact speeds were in the range 1.0 – 4.4 m/s and the drop weight was 3.47 kg. The force was logged at 100 kHz with a piezoelectric sensor.

B) Three-point bending

The test fixtures were according to ISO 178 (quasi-static tests at constant cross-head speed) and ISO 179 (falling weight impact tests). Bars with cross-section 4×10 mm^2 and length 80 mm length were tested flatwise. The span was 60 mm. For the falling weight tests, the impact speeds were in the range 1.0 – 4.4 m/s and the drop weight was 3.47 kg.

3. Simulation

The commercial finite element code LS-DYNA (ls971_d_R4.2) was used in this study. SAMP-1, which has been developed specially for polymer materials, was chosen as constitutive model.

The yield function was calibrated using tensile and compressive test data, with linear pressure dependence (Drucker-Prager). In order to use the damage parameter as a function of equivalent plastic strain, the net stress (with effect of damage) vs. plastic strain was tabulated instead of gross true stress-strain. There is an option within the SAMP-1 model to give just the measured true stress, but the automatic calculation of the net stress was not always stable. Therefore, the net stress-strain was calculated outside LS-DYNA and given as input:

$$\bar{\sigma}_{net} = \frac{\bar{\sigma}}{1 - D(\varepsilon^p)} \tag{5}$$

where $\bar{\sigma}$ and $\bar{\sigma}_{net}$ are the true and net stresses, D is the damage parameter, and ε^p is the plastic strain, which was found by iterating the equation below:

$$\bar{\sigma} = E\left[1 - D(\varepsilon^p)\right]\left[\varepsilon^{tot} - \varepsilon^p\right] \tag{6}$$

The stress-strain curve corresponding to a strain rate of 0.002 s^{-1} was used as reference, and this curve was scaled for all strain rates shown in Figure 4, for both tension and compression. Hence, the yield stresses in tension and compression were assumed to have the same strain rate dependence.

Brick elements were used for three-point bending, while an axisymmetric model was used to model plate impact. Columb friction was assumed. A friction coefficient of 0.05 was used for the lubricated surfaces, and a coefficient of 0.2 was used for the unlubricated surfaces [8].

4. Results

Some comparisons between simulated and measured responses are shown below. For three-point bending, the quasi-static test and impact tests at low loading rates are well predicted (Figure 7a and Figure 7b). However, the test at 4 m/s is underpredicted (Figure 7c). Regarding the falling weight impact of plates, the response of the 4 mm thick plate appears to be well predicted (Figure 8). The response of the 2 mm thick plate is predicted up to a certain deflection (Figure 9). Above this deflection, our model does not describe the response, nor does it predict the deformed shape of the plate after impact (Figure 10). The same deviation was also observed for the 4 mm plate at a loading rate of 4.4 m/s.

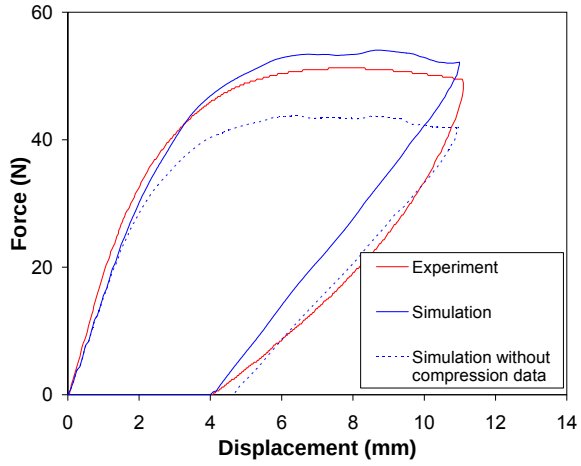

a) Constant loading rate 10 mm/min.

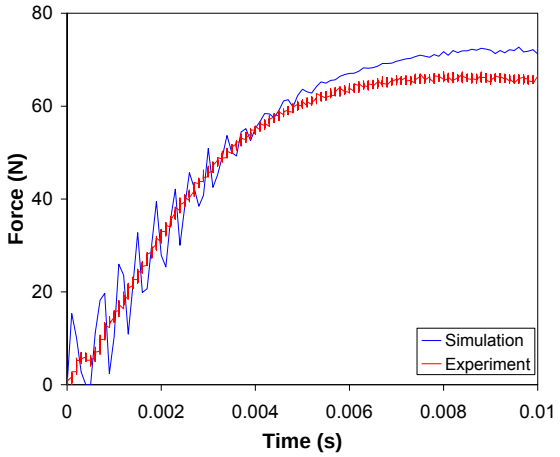

b) Falling weight impact at 1 m/s.

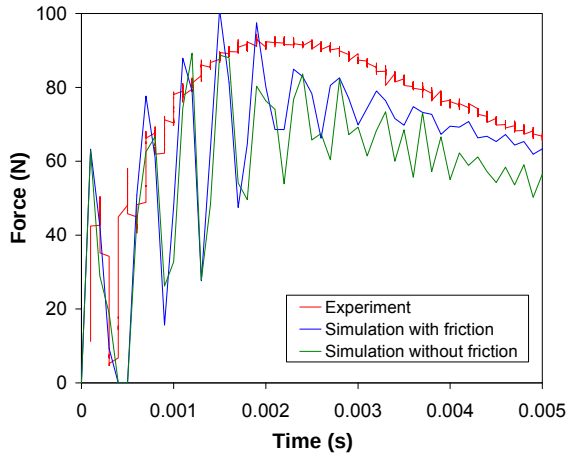

c) Falling weight impact at 4 m/s. "With friction" means friction coefficients 0.05 and 0.2 for striker and support, respectively (as in the other simulations).

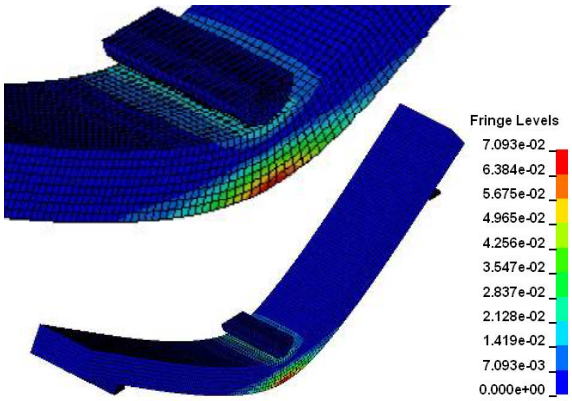

d) Effective plastic strains for falling weight impact at 4 m/s.

Figure 7: Results for three-point bending. Experimental data were obtained with bars from dogbones.

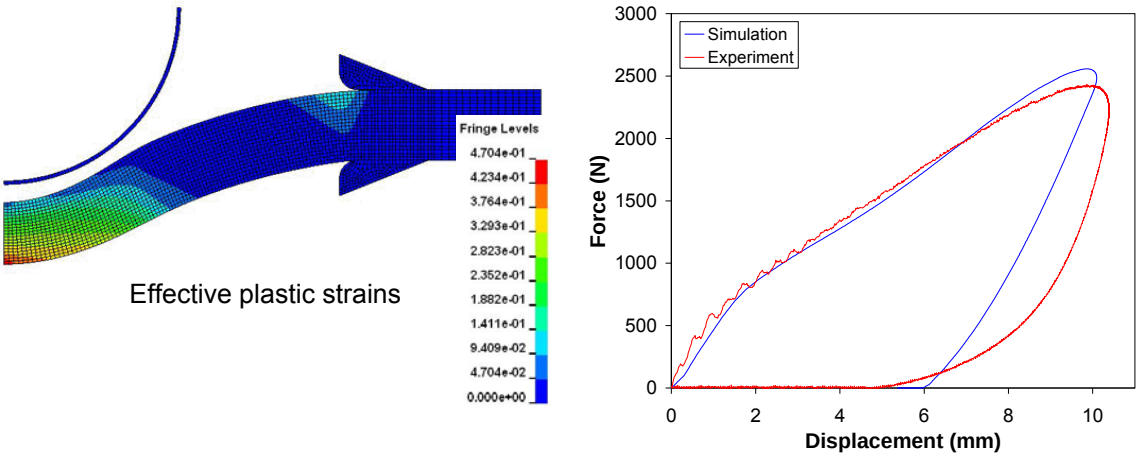

Figure 8: Falling weight impact on 4 mm thick plate. Impact speed 3 m/s.

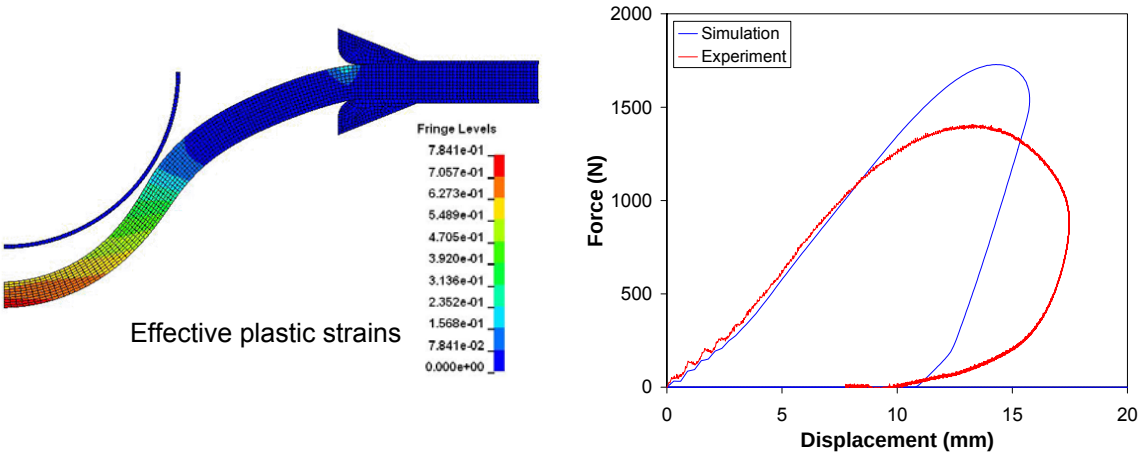

Figure 9: Falling weight impact on 2 mm thick plates. Impact speed 3 m/s.

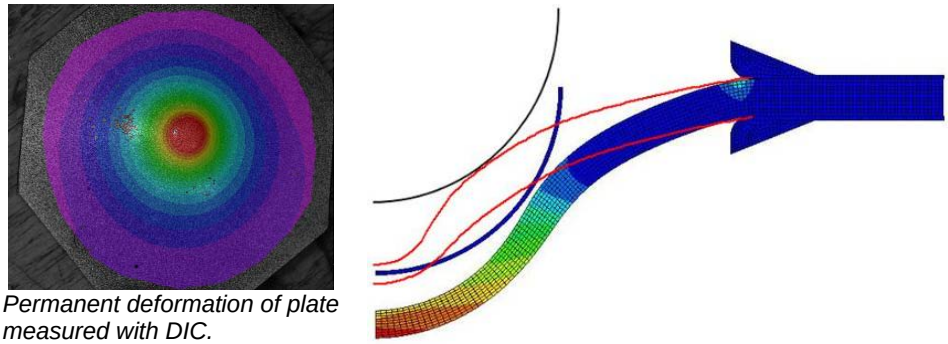

Permanent deformation of plate measured with DIC.

Figure 10: Right*: Comparison between measured (red lines, measured with DIC) and simulated cross-section of plate after impact (permanent deformation). 2 mm thick plate and impact speed 3 m/s.*

5. Discussion

Our model (not necessarily SAMP-1) is based on a number of assumptions and simplifications:

- Isotropic and homogeneous material
- No visco-elastic effects
- No thermal effects
- Same modulus in tension and compression
- Same hardening curve shape for compression and tension (only different scale factors)
- Same hardening curve shape for all strain rates (only a scale factor)
- Same strain rate effect in tension and compression, i.e. same ratio of compressive yield stress to tensile yield stress at all strain rates
- Yield surface with linear dependence on hydrostatic stress
- Damage parameter only dependent on plastic strain, not hydrostatic stress, strain rate etc
- Constant, and somewhat arbitrary, friction coefficients

We are presently looking into some of these issues, like the strain rate dependence of the compressive hardening curve, and the strain rate dependence of the damage parameter. A combination of additional tests and inverse modelling is perhaps the best approach. In addition to the list above, there are also issues related to the numerical solution that may affect the simulation results.

The simplest validation test, quasi-static three-point bending with constant loading rate, is well predicted (Figure 7a). During loading the response is slightly underpredicted at small deflections, and slightly overpredicted at larger deflections. This indicates that the compression input is somewhat too high. Poor friction modelling can also affect the prediction at large displacements. The predicted unloading is what we could expect with this model, and it is OK for many industrial applications. This three-point bending test can be a reference point for discussing the other validation tests.

For the falling weight impact three-point bending, the difference between measured and predicted responses seems to increase with increasing loading rate (Figure 7b to Figure 7c). The response is underpredicted at the highest loading rate. Hence, the strain rate dependence of the data needs to be improved. This could be yield stress and/or hardening curves for tension and/or compression. The strain rate data obtained in this study showed an approximately linear relation between yield stress and strain rate on a logarithmic scale. In the simulations it was observed that the force vs. displacement was sensitive to the yield stress input at high strain rates. The aim of this work is to predict the impact response of ductile polymers. A number of tests (e.g. ISO 18872) have been suggested for high strain rates, but there are still many open questions. The use of DIC with high-speed cameras is an important advancement. Finally, also for this validation case, the friction modelling is a source of error.

The falling weight impact loading of the 4 mm thick plate differs from the three-point bending by having biaxial stress. The strains and strain rates were somewhat lower in the former case, partly because the impact speed was lower (3 vs. 4 m/s). Also, the plate impact test has more non-linearity due to the increase in contact area between the plate and the hemispherical striker during loading. With the SAMP-1 model, the plate impact test (Figure 8) seems to be better predicted than the three-point bending impact. This is, however, probably only a coincidence. Firstly, the anisotropy of the plate was not included in the model. As shown in Figure 2, a bar cut from the plate in the direction perpendicular to flow is less stiff than a bar cut parallel to flow, and the model was calibrated with a dogbone with properties close that of the bar cut parallel to flow. Hence, our model overpredicts the bending stiffness of the plate by neglecting this anisotropy. Secondly, the material may soften in biaxial tension and also biaxial compression, compared to the uniaxial stress states, as is often the case [5]. This is only indirectly included in our model, since the yield surface is based on two points (uniaxial tension and uniaxial compression), and a higher yield stress in uniaxial compression than in uniaxial tension (as in our case) then gives a lower yield stress in biaxial tension than in uniaxial tension. However, if data for biaxial tension would show a stronger softening than our model, the present model overpredicts the response. Thirdly, we are probably still underpredicting the strain rate dependence, as for the three-point bending in Figure 7. Hence, the apparently good agreement in Figure 8 is probably due to these three effects cancelling each other.

The last validation test is the falling weight impact loading of the 2 mm thick plate. In this test the strains are larger than for the 4 mm thick plate. The stress state is also different at the highest strains. The predicted permanent deformation is quite different from the observed shape, which has more localised deformation. This fact indicates that our model is not adequate for such cases. Visco-elastic effects may be involved in this particular deformation, and thermo-mechanical effects [2] can be important at the high strain rates occuring in this plate at this loading rate. A better description of the yield surface is also needed. This should include data for shear and biaxial tension, perhaps with inverse modelling as a tool.

6. Conclusion

The SAMP-1 model is suitable for simulating the impact of ductile polymers. For our material and our test cases we need to improve the material data in terms of strain rate effects, stress state effects and anisotropy effects. Combining testing and simulation (inverse modelling) is useful for identifying and obtaining critical material parameters. In further studies we will also try to model the onset of fracture with SAMP-1.

7. Acknowledgments

The authors would like to thank the Research Council of Norway (BIA programme) and Plastal AS for financial support, and for the PhD studentship grant to Hamid Daiyan.

8. Literature

[1] Duan, Y., Saigal, A., and Greif, R., "Impact behavior and modeling of engineering polymers", Polymer Engineering and Science, vol. 43, 2003, pp. 112-124

[2] Viana, J. C., Cunha, A. M., and Billon, N., "Experimental characterization and computational simulations of the impact behavior of injection-molded polymers", Polymer Engineering and Science, vol. 47, 2007, pp. 337-346

[3] Kolling, S., Haufe, A., Feucht, M., and Du Bois, P., "SAMP-1: A Semi-Analytical Model for the Simulation of Polymers," in LS-DYNA Anwenderforum, 2005

[4] Sutton, M. A., McNeill, S. R., Helm, J. D., and Chao, Y. J., "Advances in two-dimensional and three-dimensional computer vision," in *Photo-Mechanics*. vol. 77 Berlin: Springer-Verlag Berlin, 2000, pp. 323-372

[5] Temimi-Maaref, N., Burr, A., and Billon, N., "Damaging processes in polypropylene compound: Experiment and modeling", Polymer Science Series A, vol. 50, 2008, pp. 558-567

[6] Du Bois, P. A., Kolling, S., Koesters, M., and Frank, T., "Material behaviour of polymers under impact loading," in International Symposium on the Crashworthiness of Light-Weight Automotive Structures, Trondheim, NORWAY, 2004

[7] Schrauwen, B. A. G., Janssen, R. P. M., Govaert, L. E., and Meijer, H. E. H., "Intrinsic deformation behavior of semicrystalline polymers", Macromolecules, vol. 37, 2004, pp. 6069-6078

[8] Crocker, L. and Dean, G., "Prediction of impact performance of plastics mouldings, part 2: Finite element simulations", Plastics, Rubber and Composites, vol. 36, 2007, pp. 14-25